Colloids and Surfaces B: Biointerfaces 154 (2017) 55–62

Contents lists available at ScienceDirect

Colloids and Surfaces B: Biointerfaces

journal homepage: www.elsevier.com/locate/colsurfb

Shape-dependent enzyme-like activity of Co_3O_4 nanoparticles and their conjugation with his-tagged EGFR single-domain antibody

Wei Zhang[a,b,1], Jinlai Dong[a,1], Yang Wu[c], Peng Cao[d,e], Lina Song[a,b], Ming Ma[a,b], Ning Gu[a,b,*], Yu Zhang[a,b,*]

[a] State Key Laboratory of Bioelectronics, Jiangsu Key Laboratory for Biomaterials and Devices, School of Biological Science and Medical Engineering, Southeast University, Nanjing 210096, PR China
[b] Collaborative Innovation Center of Suzhou Nano Science and Technology, Southeast University, Nanjing 210096, PR China
[c] Research Centre of Clinical Oncology, Jiangsu Cancer Hospital, Nanjing 210009, PR China
[d] Hospital of Integrated Traditional Chinese and Western Medicine, Nanjing University of Chinese Medicine, Nanjing 210028, PR China
[e] Laboratory of Cellular and Molecular Biology, Jiangsu Province Academy of Traditional Chinese Medicine, Nanjing 210028, PR China

ARTICLE INFO

Article history:
Received 11 April 2016
Received in revised form 17 February 2017
Accepted 27 February 2017
Available online 28 February 2017

Keywords:
Co_3O_4 nanoparticles
Peroxidase
Crystal plane
His-Tag
Immunohistochemistry

ABSTRACT

In this study, Co_3O_4 nanopolyhedrons, nanocubes, nanoplates and nanorods were synthesized and characterized. Furthermore, the peroxidase- and catalase-like activities of these Co_3O_4 nanoparticles (NPs) were studied and influence of the exposed crystal planes was explored. According to their morphology and peroxidase-like activity, dimercaptosuccinic acid (DMSA) modified Co_3O_4 nanopolyhedrons synthesized via coprecipitation method (Co_3O_4 NHs) were selected as a proper candidate for the immunohistochemical (IHC) detection of epidermal growth factor receptor (EGFR) expression in non-small cell lung cancer (NSCLC) tissues. Bivalent cobalt ions were coupled to the carboxyls on the surface of the obtained Co_3O_4 NHs so as to chelate the hexahistidine residues (His-Tags) at the C-terminal of EGFR single-domain antibodies (EGFR sdAbs). Finally, the as-obtained EGFR sdAbs-binding Co_3O_4 NHs (Co_3O_4 nanoprobes) were successfully applied to the detection of EGFR expression in NSCLC tissues.

1. Introduction

Nowadays with the rapid development of the synthesis and characterization techniques, nano-catalysts are no longer considered simply as the stack of inorganic crystals, instead, the catalytic activity and specificity are being researched at the layer of atomic level and crystal structure [1–9]. Bratlie et al. [1] reported the structure-dependent surface chemistry of benzene hydrogenation on Pt (100) and Pt (111) single-crystal surfaces, the former catalyzed only the formation of cyclohexane while the latter contributed to cyclohexene production besides cyclohexane. Tian et al. [2] found that in the electro-oxidation processes of small organic fuels such as formic acid and ethanol, platinum nanoparticles (PtNPs) with high-index facets including (730), (210) and (520) exhibited higher catalytic activity than PtNPs with stable facets such as (111), (100) and (110). Narayanan et al. [3] studied the electron-transfer reaction between hexacyanoferrate(III) ions and thiosulfate ions in colloidal solutions mainly containing tetrahedral, cubic or near spherical PtNPs as catalysts. The results show that the catalytic activity of these PtNPs hinges on the fraction of Pt atoms located at corners and edges of each surface. Besides PtNPs, studies on the relationship of crystal facets exposure and the catalytic activity of all kinds of nanoparticles (NPs) have also been presented [4–8].

As a kind of p-type semiconductor material, Co_3O_4 continues to be of great interest due to its excellent physical and chemical properties, which have been extensively exploited in the areas of magnetics, photology, electronics and catalysis [10,11]. Our previous study [12] indicated that Co^{3+} plays the chief role in the catalytic behavior of Co_3O_4 NPs. In this study, the relationship between the catalytic activity of Co_3O_4 NPs and the exposed crystal planes containing different density of Co^{3+} was discussed. For this, Co_3O_4 nanoplates, nanopolyhedrons, nanorods and nanocubes with different exposed crystal faces were selectively synthesized and their peroxidase- and catalase-like activities were investigated.

Contrast to conventional V_H (variable domains of heavy chain)-V_L (variable domains of light chain) paired antibody, single-domain

* Corresponding authors at: State Key Laboratory of Bioelectronics, Jiangsu Key Laboratory for Biomaterials and Devices, School of Biological Science and Medical Engineering, Southeast University, Nanjing 210096, PR China.
E-mail addresses: guning@seu.edu.cn (N. Gu), zhangyu@seu.edu.cn (Y. Zhang).
[1] These authors contributed equally to this work.

http://dx.doi.org/10.1016/j.colsurfb.2017.02.034
0927-7765/

antibody (sdAb) has some advantages including enhanced stability, reduced size, improved solubility, facile structure variations, ability of recognizing small hidden antigenic sites, enzyme inhibition, higher production yield, shorter serum half-life and lower immunogenicity [13–17]. In our study, an antibody conjugation method was developed taking use of the chelation between the hexahistidine residues (His-Tags) at the C-terminus of epidermal growth factor receptor (EGFR) sdAbs and divalent cobalt ions coated on the surface of Co_3O_4 NPs. Finally, the obtained Co_3O_4 nanoprobes were applied on the immunohistochemistry (IHC) detection of EGFR expression of non-small cell lung cancer (NSCLC) tissues.

2. Experimental section

2.1. Reagents and materials

All chemicals used in the experiment were analytical grade reagent and were used as received. 2, 2′-azinobis (3-ethylbenzo-thiozoline) −6-sulfonic acid (ABTS), 3, 3′, 5, 5′-tetramethylbenzidine (TMB) and 30% H_2O_2 were obtained from Sigma-Aldrich. Dimethyl sulfoxide (DMSO), glacial acetic acid, anhydrous sodium acetate, sodium hydroxide, ethanol, glycol and acetone were purchased from Sinopharm Chemical Reagent Co., Ltd. Cobalt(II) nitrate ($Co(NO_3)_2{\cdot}6H_2O$) and oleylamine were obtained from Aladdin Co. Ltd. 5-Cl-PADAB was brought from Tokyo Chemical Industry Co., Ltd. Urea ($CO(NH_2)_2$) was brought from Xilong Chemical Co., Ltd. Ammonia water, dimercaptosuccinic acid (DMSA), sodium dodecyl benzene sulfonate (SDBS), citric acid, glacial acetic acid, boric acid, anhydrous sodium sulfate, sodium tetraborate and octanol were reagents from Shanghai Ling Feng Chemical Reagent Co., Ltd. Hydrochloric acid was produced by Nanjing Chemical Reagent Co., Ltd. Albumin bovine (BSA) was obtained from Nanjing Bookman Biotechnology Co., Ltd. Hematoxylin, pepsin and Diaminobenzidine (DAB) were produced by Fuzhou Maixin Biotechnology Development Co., Ltd. BCA Protein Assay Kit was produced by KeyGEN BioTECH Co., Ltd. Deionized water used throughout all experiments was purified with the Millipore system.

2.2. Synthesis of Co_3O_4 nanopolyhedrons via coprecipitation method

Co_3O_4 nanopolyhedrons were prepared via coprecipitation method described by Wang [18] with some minor modifications. Firstly, mix 50 mL of $Co(NO_3)_2{\cdot}6H_2O$ (20 mM) with 0.84 mL ammonia water, add 60 μL 30% H_2O_2 into the mixture under 1000 rpm stirring at 60 °C and add 20 mL of $Co(NO_3)_2{\cdot}6H_2O$ (10 mM) immediately to react for 3 h. Then the precipitate was separated by centrifugation at 9000 rpm for 20 min and then washed with pure water for three times. Next, dissolve the product in pure water and adjust the pH of the solution to 2 before adding 0.045 g of DMSA (in 1 mL DMSO) under ultrasonic stirring for 30 min, and then mechanically stir the solution for 3 h, adjust pH of the solution to 9 and disperse the solution until it becoming clear with by ultrasonic dispersing technology. Finally, adjust pH of the solution to 7 and purify the NPs via dialysis using cellulose dialysis tubing (MWCO 13000, Viskase Co., USA).

2.3. Synthesis of Co_3O_4 nanopolyhedrons via solvothermal method

Co_3O_4 nanopolyhedrons were synthesized via solvothermal method referring Duan's method [10]. 1.0 g of $Co(NO_3)_2{\cdot}6H_2O$ was dissolved in 22 mL *n*-octyl alcohol, 3.3 g of SDBS was added to react for 30 min under magnetic stirring, the solution was then moved to a high temperature high pressure reactor in a muffle furnace and reacted at 90 °C for 6 h and then at 200 °C for 48 h. After that, 15 mL of hexane, 10 mL of ethanol and 25 mL of pure water were added to the solution in the previous step for the extraction of oil phase Co_3O_4. Finally the precipitation was separated with centrifugation and pure Co_3O_4 nanopolyhedrons were obtained after getting rid of organic impurities in the precipitation via calcining at 350 °C.

2.4. Synthesis of Co_3O_4 nanocubes

Co_3O_4 nanocubes were synthesized according to Li's method [11]. 0.04 mmol of $Co(NO_3)_2{\cdot}6H_2O$ was dissolved in 40 mL of pure water and mixed with 0.01 mmol of NaOH, and then the obtained violet solution was added in a high temperature high pressure reactor and reacted at 180 °C for 5 h. When cooled to room temperature, the precipitation was washed with pure water and ethanol for three times, respectively. Finally, the precipitation was resuspended in 10 mL of ethanol.

2.5. Synthesis of Co_3O_4 nanoplates

Co_3O_4 nanoplates were also synthesized according to Li's method [11]. Mixture of 20 mL of $Co(NO_3)_2{\cdot}6H_2O$ (50 mM), 2 mL of oleylamine and 10 mL of enthanol was stirred under magnetic stirring for 30 min. Then the solution was moved to a high temperature high pressure reactor in a muffle furnace and reacted at 180 °C for 48 h, the product was washed with ethanol for 3 times. Finally, the power was calcined at 350 °C for 3 h to get the end-product.

2.6. Synthesis of Co_3O_4 nanorods

Co_3O_4 nanorods were prepared according to Zeng's method [19]. 1.92 g of $Co(NO_3)_2{\cdot}6H_2O$ and 4 g of $CO(NH_2)_2$ was dissolved in 20 mL of pure water and placed into a high temperature high pressure reactor in a 90 °C muffle furnace to react for 20 h. Next, the obtained precipitation was dried at 50 °C in an oven. Finally, Co_3O_4 nanorods were obtained via calcining the precipitation at 450 °C for 3 h.

2.7. Characterization

The size and morphology of Co_3O_4 NPs were determined by transmission electronic microscopy (TEM, JEOL JEM-2100). Samples were dropped onto a carbon-coated copper grid and dried at room temperature and characterized using TEM. Electronic diffraction (ED) was used to determine the crystalline structure of the obtained NPs. X-ray diffraction (XRD) data were collected with a diffractometer (ARL X'TRA). Ultraviolet visible (UV-vis) absorption spectra were recorded on an UV–vis spectrophotometer (Shimadzu UV-3600).

2.8. Cobalt concentration detection of Co_3O_4 NPs

Coloring spectrophotometric determination of Cobalt concentration was operated via 4-(5-chloro-2-pyridyl)-azo-1,3-diaminobenzene (5-Cl-PADAB) method [20,21]. Firstly, a standard curve was set up according to the absorbance of $Co(NO_3)_2$ aqueous solution of different concentration; more narrowly, 20 μL, 40 μL, 60 μL, 80 μL and 100 μL of 1 mg/mL $Co(NO_3)_2$ solution was mixed respectively with 5 mL of citric acid (0.45 M), 2 mL of ammonium hydroxide (13%) and 5 mL of sodium acetate (10%). 1 mg/mL 5-Cl-PADAB ethanol solution was then added and the mixture was incubated at 80 °C for 10 min. When cooled to room temperature, 15 mL of sulfuric acid solution (25%) was added. The solution was diluted to 50 mL with pure water and absorption at 570 nm was measured. Secondly, Cobalt concentration in Co_3O_4 NPs was measured using the same method. In brief, some Co_3O_4 NPs was

dissolved in 1 mL of hydrochloric acid (6 M) by an ultrasonic method and mixed with 5 mL of citric acid (0.45 M), and then a reasonable amount of ammonium hydroxide (13%) was used to adjust pH to 8. Finally, 5-Cl-PADAB method was employed to finish the detection as previously mentioned. Cobalt concentration was calculated according to the absorbance at 570 nm.

2.9. Peroxidase-like activity detection

Co_3O_4 NPs were dispersed in pure water and adjusted to a concentration of 0.1 mg/mL. 10 μL of Co_3O_4 NPs (0.1 mg/mL) were mixed with 200 μL of acetate buffer (0.2 M, pH 3.6), 10 μL of TMB (10 mg/mL in DMSO) and 32 μL of H_2O_2 (30%). The absorbance values of the reaction systems catalyzed by Co_3O_4 NPs were recorded at each 30 s for 2 min with a microplate reader [12,22]. Reaction velocity was calculated via linear fitting the absorbance and time.

2.10. Catalase-like activity detection

The catalytic reaction was performed in the PBS buffer (pH 7.4). Briefly, adding 50 μL of Co_3O_4 NPs (0.1 mg/mL) in 4.5 mL of PBS buffer (pH 7.4) in presence of 0.5 mL of H_2O_2 (30%). The generated oxygen in the reaction systems were measured by multi-parameter analyzer (DZS-708) at every 1 min for 4 min [12,23].

2.11. Conjugation of Co_3O_4 NHs and the His-Tag fused EGFR sdAbs

A recombinant protein named EGFR sdAbs consisting of an anti-EGFR VHH (the variable domain from the heavy chain of the antibody) with a His-Tag placed at the C-terminus was provided by Cao's group [24]. Incubate 1 mL DMSA coated Co_3O_4 NHs (0.01 mg/mL) with different volume (1, 2.5, 5, 10, 50, 100, 200 μL) of 10 mg/mL $Co(NO_3)_2{\cdot}6H_2O$ for 30 min to fulfill the adsorption of Co^{2+}. Zeta potential of Co_3O_4 NHs was detected to determine the optimal adsorption quantity. Incubate 1 mL of the optimal Co^{2+} adsorbed Co_3O_4 NHs with different volume (20, 40, 60, 80, 100 μL) of His-Tag fused EGFR sdAbs (0.92 mg/mL) for 30 min and then centrifuge the sample to remove the free sdAbs. Finally, block the nanoprobes with 100 μL of BSA solution (10%) for the following IHC detection.

2.12. Quantitative analysis of antibody content in the nanoprobes

Centrifuge the nanoprobes at 10000 rpm for 30 min at 4 °C to separate the conjugated sdAbs and the free ones. The antibody concentration in the supernatant was determined using a BCA kit [25]. The amount of antibody conjugated to Co_3O_4 NHs was the difference value of total antibody amount and the antibody in the supernatant.

2.13. IHC assay

IHC experiments were performed using NSCLC tissue sections to detect EGFR overexpressed tumor cells [12,15,26,27]. The NSCLC tissue slides used in this study were obtained from Zhongda hospital with a clinical report of EGFR expression for reference. One experiment group and three control groups were set in each NSCLC tissue to validate that Co_3O_4 nanoprobes can be served as a useful probe. Paraffin sections were deparaffinized by submerged in dimethylbenzene for three times; each for 10 min, then rehydrated the sections using graded ethanol (100%, 100%, 90%, 80%, 70%) and distilled water, each socked for 10 min. After that the tissue sections were moved into a wet box, the water around the tissues was wiped off and the tissues were incubated with 3% H_2O_2 for 15 min in darkness to block the endogenous peroxidase (EGPO) activity. The sections were submerged in PBS (pH 7.4) for 3 times after the residual H_2O_2 was washed off with distilled water. The fluid around the tissues were wiped off, proper amount of pepsin was added on the tissues which were then incubated at 37 °C for 30 min. The tissue sections were washed for three times with PBS, each for 5 min, and then in a wet box the tissues were blocked with 1% BSA at for 20 min 37 °C, washed with PBS as described before. Afterwards, group 1 (EGFR positive NSCLC tissue) and group 4 (EGFR negative NSCLC tissue) were incubated with Co_3O_4 nanoprobes at 37 °C for 30 min, group 2 (EGFR positive NSCLC tissue) was blocked with 0.92 mg/mL EGFR sdAb at 37 °C for 30 min and then incubated with Co_3O_4 nanoprobes at 37 °C for 30 min, group 3 (EGFR positive NSCLC tissue) was incubated with Co_3O_4 NHs at 37 °C for 30 min. All of the sections were treated with freshly prepared DAB for 20 min after recovering at room temperature for 1 h and washed with PBS for three times, they were counterstained with hematoxylin (blue stain) after washed with PBS, then the sections were dehydrated with an ethanol gradient (70%, 80%, 90%, 100%, 100%), each for 10 min. And then the slides was washed twice with xylene, each for 10 min, the sections were then sealed with coverslip using neutral balsam. Finally, the stained sections were observed under a microscope.

3. Results and discussion

3.1. Characterization of Co_3O_4 nanopolyhedrons-CP

As shown in Fig. 1a and b, the as-prepared Co_3O_4 nanopolyhedrons-CP have irregular polyhedral morphology. The XRD pattern of Co_3O_4 nanopolyhedrons-CP can be indexed to (111), (220), (311), (222), (400), (422), (511) and (440), which is in accord with the reported data of Co_3O_4 [28–30] (Fig. S1). The electron diffraction (ED) pattern also displays (440), (511), (400), (311) and (220) crystal planes (Fig. S2a). The d spaces calculated according to the ED patterns are 0.468 nm for (111) plane, 0.286 nm for (220) plane and 0.234 nm for (222) plane. These results indicate that the obtained nanopolyhedrons are a cubic spinel phase of Co_3O_4 (JCPDS No. 43-1003). Fig. S2b and c demonstrates (220) planes at a 35° angle and (222) planes at a 60.5° angle from the (111) planes. Therefore, (110) plane is the dominating crystal plane exposed in Co_3O_4 nanopolyhedrons-CP because it is perpendicular to all the crystal planes shown in Fig. S2b and c [11]. UV–vis spectrum (Fig. S3, blue line) shows two absorption peaks in the wavelength ranges of 200–300 nm and 400–550 nm. The foregoing peak concerns O^{2-}-Co^{2+} charge transfer while the latter is correlated with O^{2-}-Co^{3+} charge transfer [31,32].

3.2. Characterization of Co_3O_4 nanocubes

TEM images (Fig. 1c, d) show regular cubic Co_3O_4 nanocubes, whose size distributes in the range of 200–500 nm. The XRD pattern (Fig. S1) of the obtained Co_3O_4 nanocubes is in accord with the reported data of Co_3O_4. ED pattern (Fig. S2d) displays perpendicular (220) planes and (400) planes. HR-TEM images (Fig. S2e, f) show mutually perpendicular (220) planes and 45° angle crossed (440) and (220) planes. Thus we inferred Co_3O_4 nanocubes expose (100) planes.

3.3. Characterization of Co_3O_4 nanoplates

As shown in Fig. 1e, the as-prepared Co_3O_4 nanoplates (without calcination) present hexagonal morphology and their size ranging from 0.5 to 2.5 μm. The black thin strips are vertically oriented nanoplates, indicating their thickness is within 150 nm. To prevent the impurities on the surface of Co_3O_4 nanoplates from inhibiting the affinity to enzyme substrates, the obtained Co_3O_4 nanoplates

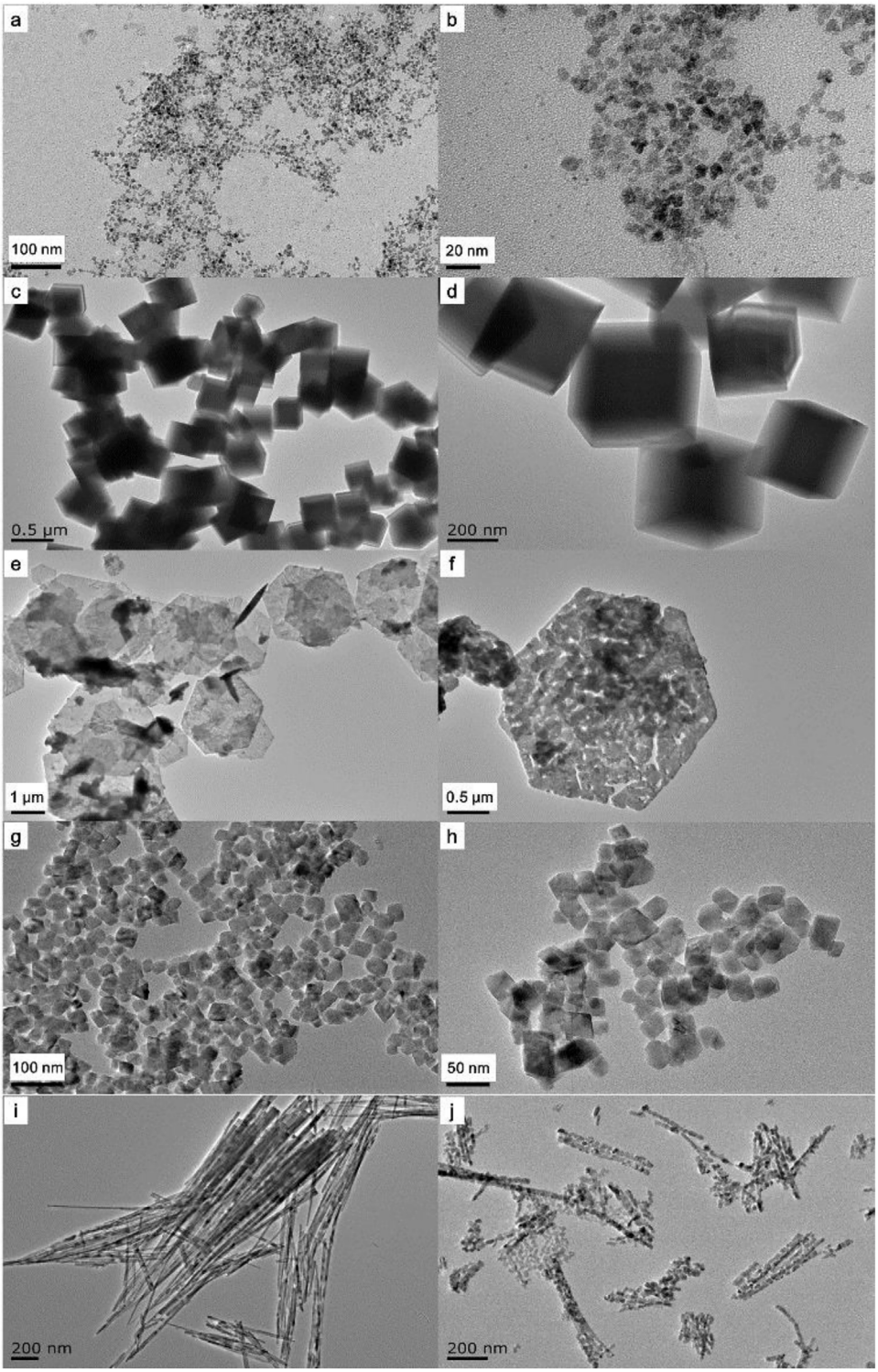

Fig. 1. TEM images of (a, b) Co_3O_4 nanopolyhedrons-CP, (c,d) Co_3O_4 nanocubes, (e) Co_3O_4 nanoplates before calcination, (f) Co_3O_4 nanoplates after calcination, (g, h) Co_3O_4 nanopolyhedrons-ST, (i) Co_3O_4 nanorods before calcination, and (j) Co_3O_4 nanorods after calcination.

were calcined to remove the organics. The holes (Fig. 1f) appeared in the Co_3O_4 nanoplates offered larger contact area for the enzyme substrates and H_2O_2 [18]. In addition, the by-product β-$Co(OH)_2$ (Co^{2+}) was transformed into Co_3O_4 ($Co^{3+/2+}$) after the calcination. For these reasons, the catalytic activity could be greatly promoted via calcination. The XRD pattern (Fig. S1) of these Co_3O_4 nanoplates is in keeping with the reported data of Co_3O_4. ED pattern (Fig. S2g) shows (111), (220) and (311) planes. HR-TEM images (Fig. S2h, i) show mutually perpendicular (220) and (222) planes, indicating the exposed crystal plane of Co_3O_4 nanoplates is (112), which is perpendicular to both (220) and (111) planes.

3.4. Characterization of Co_3O_4 nanopolyhedrons-ST

TEM image of the Co_3O_4 nanopolyhedrons-ST (Fig. 1g and h) contains irregular cubic or polyhedral nanoparticles (Fig. S5b). The

Table 1
Peroxidase- and catalase-like activities of the five kinds of Co_3O_4 NPs.

Co_3O_4 NPs	exposed crystal planes	peroxidase-like activity (U/μg Co_3O_4)	catalase-like activity (U/μg Co_3O_4)
Co_3O_4 nanoplates	(112)	0.031	3.23
Co_3O_4 nanopolyhedrons-CP	(110)	0.018	2.70
Co_3O_4 nanopolyhedrons-ST	(110)	0.016	2.32
Co_3O_4 nanorods	(110) and (111)	0.012	1.33
Co_3O_4 nanocubes	(100)	0.006	0.92

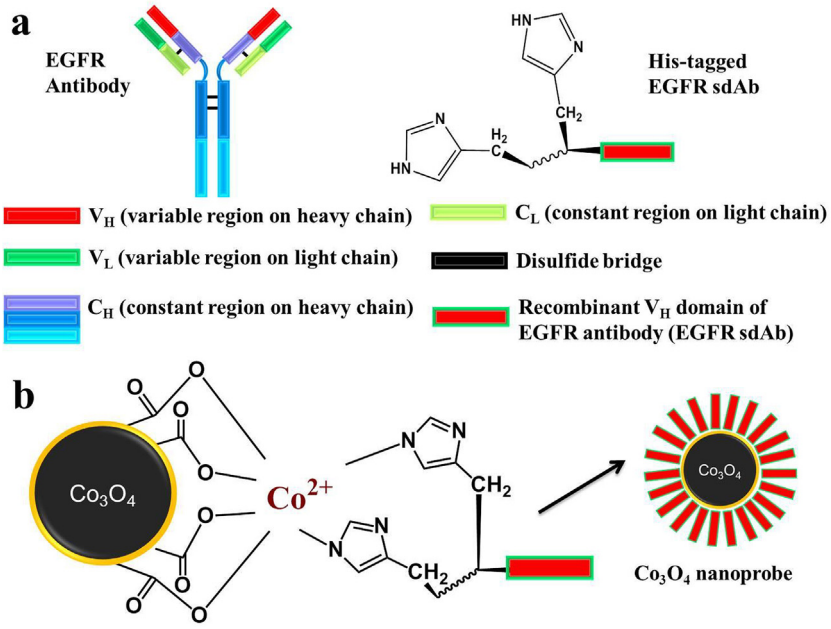

Scheme 1. Scheme representation of the preparation of Co_3O_4 nanoprobes. (a) Illustration of His-tagged EGFR sdAb. (b) Construction of Co_3O_4 nanoprobes.

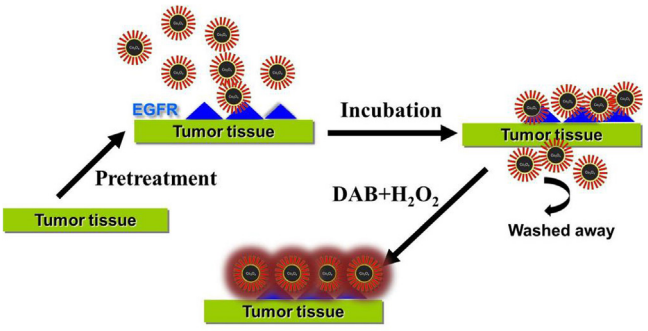

Scheme 2. IHC assay taking use of the high peroxidase-like activity of Co_3O_4 nanoprobes.

XRD pattern (Fig. S1) of these Co_3O_4 nanopolyhedrons-ST is in accord with the reported data of Co_3O_4. ED pattern (Fig. S2j) reveals (220), (311), (400), (511) and (440) planes, which is in consistence with cubic spinel phase of Co_3O_4 (JCPDS No. 43-1003). 60.5° angle crossed (111) planes were observed in HR-TEM images (Fig. S2k and l), showing that similarly to Co_3O_4 nanopolyhedrons-CP, Co_3O_4 nanopolyhedrons-ST also expose (110) planes. UV–vis spectrum (Fig. S3) of Co_3O_4 nanopolyhedrons-ST fits with the absorption feature of Co_3O_4 nanopolyhedrons-CP.

3.5. Characterization of Co_3O_4 nanorods

The precursors (Co_3O_4 nanorods without calcination) of Co_3O_4 nanorods showed rod-like structures with the diameter ranging from 10 nm to 20 nm while the length is in the range of 0.5 μm–2 μm (Fig. 1i). The main composition of the precursors is $Co(OH)_x(CO_3)_{0.5(2-x)}$ according to the reported references [19]. $Co(OH)_x(CO_3)_{0.5(2-x)}$ was transformed to Co_3O_4 after calcination. Moreover, the calcining process removed many components from the precursors and caused the reduction in length and appearance of small gaps, as shown in TEM image (Fig. 1j). The XRD pattern (Fig. S1) of these Co_3O_4 nanorods fits the reported data of Co_3O_4. The brightest crystal planes in ED pattern (Fig. S2m) are (111) and (222), indicating the axial direction of Co_3O_4 nanorods is (111) plane, hence the exposed plane on the ends of Co_3O_4 nanorods is (111). HR-TEM results (Fig. S2n and o) of side face show 35° angle crossed (111) and (220) planes, hinting the exposed crystal plane on the side surface of Co_3O_4 nanorods is (110).

3.6. Study of peroxidase- and catalase-like activities

To obtain higher catalytic activity, we studied the relationship between catalytic activity and the crystal planes of Co_3O_4 NPs. Fig. S4a gives the peroxidase-like activity of the as-obtained five kinds of Co_3O_4 NPs, demonstrated as curves of oxidized TMB absorbance versus time. Fitting linearly, the velocities were 0.038, 0.019, 0.016, 0.012 and 0.007 for Co_3O_4 nanoplates, nanopolyhedrons-CP, nanopolyhedrons-ST, nanorods and nanocubes, respectively. Fig. S4b shows catalase-like activity curves, as function of dissolved oxygen concentration versus time. The reaction rates were 4.30, 2.16, 1.94, 1.08 and 0.97 mg L^{-1} min^{-1} for Co_3O_4 nanoplates, nanopolyhedrons-CP, nanopolyhedrons-ST, nanorods and nanocubes, respectively. To study the peroxidase- and catalase-like activities of the five kinds of Co_3O_4 NPs directly and accurately, we introduced the concept of "enzyme unit" [33]. Definition of enzyme unit (U) is the necessary amount of enzyme to catalyze

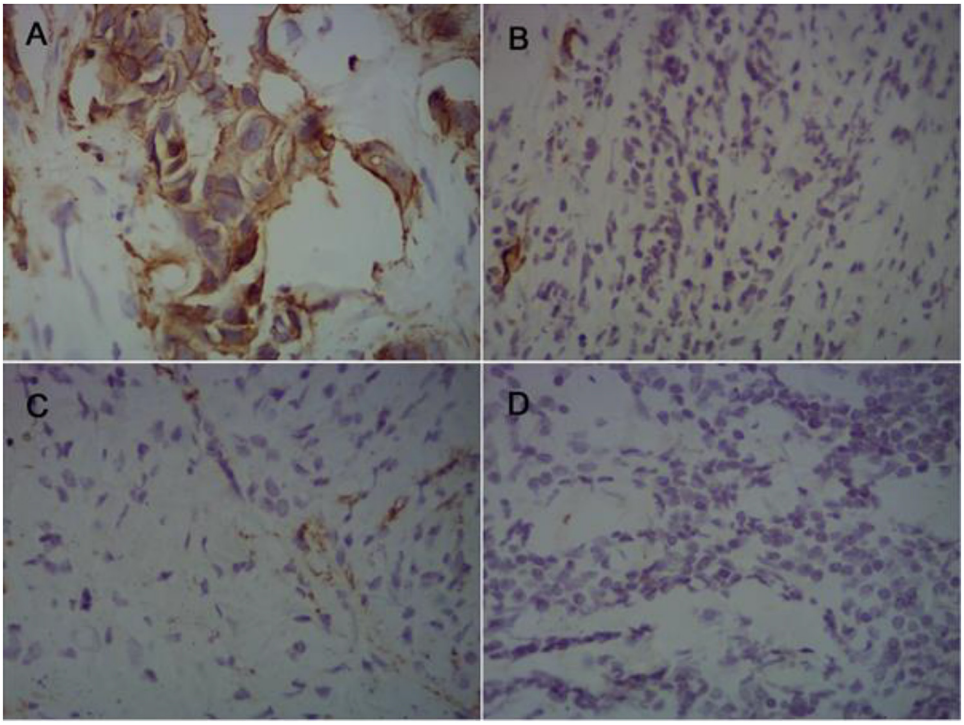

Fig. 2. Microscope images of IHC detection results. (a) EGFR positive NSCLC tissue detected using Co_3O_4 nanoprobes (400×). (b) EGFR positive NSCLC tissue detected using Co_3O_4 nanoprobes when simultaneously competed with high concentration of EGFR sdAb (100×). (c) EGFR positive NSCLC tissue detected using Co_3O_4 NHs (100×). (d) EGFR negative NSCLC tissue detected using Co_3O_4 nanoprobes (100×).

1 μmol of enzyme substrate per minute in a certain condition. The quantity of enzyme unit contained in a unit mass of enzyme reflects its catalytic activity (U/μg enzyme). Thus the peroxidase- and catalase-like activities can be evaluated according to Eqs. (1) and (2).

$$E_{POD} = \frac{A}{\varepsilon \times \mathrm{L}} \times V/m \quad (1)$$

$$E_{CAT} = \frac{DO \times V}{M} \times 2/m \quad (2)$$

E_{POD} and E_{CAT} refer to the quantity of enzyme unit per μg Co_3O_4 NPs, A is absorbance of oxidized TMB products (at 650 nm) generated per minute, ε is to molar absorption coefficient (39000 M^{-1} cm^{-1}), L is length of optical path, V is the volume of reaction solution, m is the mass of enzyme, DO represents dissolve oxygen concentration generated per minute and M is molecular weight of oxygen. The calculated results of the five kinds of Co_3O_4 NPs are presented in Table 1.

It has been shown that the acreage enclosed by the cobalt atoms in (112), (100) and (110) planes is $\left(1/2\right)a^2$, $\left(\sqrt{2}/2\right)a^2$ and $\left(\sqrt{3}/2\right)a^2$, respectively. Therefore, (112) plane is the most open and active among these three planes. [11] Because Co^{3+} plays the chief role in the catalytic behavior of Co_3O_4 NPs, [12] exposing more Co^{3+} on the surface of Co_3O_4 NPs is a beneficial way to enhance their catalytic activity. As shown in the literatures, [33,34] (111) and (100) planes do not contain any Co^{3+} while each (110) plane contains 5 Co^{2+} and 4 Co^{3+}. (111) plane contains more Co^{2+} than (100) plane. Considering the above analysis, the catalytic activity of Co_3O_4 NPs corresponding to the crystal planes follows (112) > (110) > (111) > (100) order, fitting well with our results shown in Table 1, which shows Co_3O_4 nanoplates with exposed (112) plane possess the highest catalytic activity. The catalytic activities of the (110) planes exposed Co_3O_4 nanopolyhedrons-CP and Co_3O_4 nanopolyhedrons-ST are similar, the former is slightly stronger due to the smaller size of the nanopolyhedrons (Fig. S5). The results show that Co_3O_4 nanorods expose active (110) plane on their side surface and less active (111) planes on the end surface, hence their catalytic activity is higher than (100) plane exposed Co_3O_4 nanocubes and lower than (110) plane exposed Co_3O_4 nanopolyhedrons.

3.7. Coupling of EGFR sdAbs and Co_3O_4 NHs

Considering both the catalytic activity and morphology of the five Co_3O_4 NPs, Co_3O_4 nanopolyhedrons-CP were selected as a candidate to establish a new conjugation method. The as-prepared Co_3O_4 nanopolyhedrons-CP were termed as Co_3O_4 NHs for convenience. The synthesis of Co_3O_4 NHs underwent a burst nucleation stage and a growth stage, which were not well separated and controlled so that the as-obtained Co_3O_4 NHs show irregular shapes and the crystal growth rates in different directions were not fully consistent. Therefore, abundant vacancies and bare atoms formed in the crystals, which promotes the affinity of Co_3O_4 NHs with the substrates and thereby increases their catalytic activity.

In 1975, Porath [35] introduced immobilized metal ions affinity chromatography (IMAC) taking use of the affinity of the His-Tag to metal ions including Cu^{2+}, Co^{2+}, Ni^{2+} ions. IMAC was then widely used in separation and purification of His-Tag fused recombinant proteins. Identically, the gene of EGFR sdAb was fused in frame with a series of nucleotides encoding His-Tag (Scheme 1a). Co_3O_4 NHs were conjugated with EGFR sdAbs taking advantage of the specific coordination ability between Co^{2+} and His-Tag. As shown in Scheme 1b, Co^{2+} adsorbing on the surface carboxyl goups of Co_3O_4 NHs allows the chelation of His-Tags of sdAbs. Co_3O_4 NHs were negatively charged due to the carboxyl on their surface and the absolute value of zeta potential decreased when chelated by the positively charged Co^{2+} (Fig. S6). When adding more than 5 μL Co^{2+} (10 mg/mL $Co(NO_3)_2{\cdot}6H_2O$), Co_3O_4 NHs became instable due to the insufficient electrostatic repulsion induced by the low Zeta potential (the absolute value is lower than 15 mV). Finally, 5 μL $Co(NO_3)_2{\cdot}6H_2O$

(10 mg/mL) was incubated with 1 mL Co_3O_4 NHs to prepare Co^{2+} chelated Co_3O_4 NHs.

Table S1 shows the quantitative analysis of EGFR sdAbs coupling ratio. 18.4 μg sdAbs were all conjugated to Co_3O_4 NPs because there was almost no residual sdAbs in the supernatant. When the weight of sdAbs goes higher than 36.8 μg, the amount of coupling sdAbs remained at approximately 27 μg, indicating 10 μg at most Co_3O_4 NPs (in cobalt mass) can be coupled with approximately 27 μg sdAbs. The number of EGFR sdAbs coupled on each Co_3O_4 NP can be calculated according to the following equations.

$$m_{NP} = \frac{4}{3}\pi r^3 \times \rho = 1.097 \times 10^{-18} g \quad (3)$$

$$n_{NP} = \frac{13.62 \times 10^{-6}}{m_{NP}} = 1.241 \times 10^{13} \quad (4)$$

$$n_{Ab} = \frac{27 \times 10^{-6}}{M_{Ab}} \times N_A = 1.083 \times 10^{15} \quad (5)$$

$$\text{Couplingratio} = \frac{n_{Ab}}{n_{NP}} = 87 \quad (6)$$

Co_3O_4 NHs were approximated as spheres. m_{NP} refers to mass of one Co_3O_4 NH, r is the average radius of a single Co_3O_4 NH (3.5 nm), ρ is the density of Co_3O_4 NHs (6.11 g/cm^3), n_{NP} and n_{Ab} represent number of Co_3O_4 NHs and EGFR sdAbs, M_{Ab} is molecular weight of EGFR sdAb (15 kD), while N_A is Avogadro's constant. The mass of Co_3O_4 NPs in the reaction system is 13.62 μg, whose cobalt content is 10 μg. Calculations indicate that 87 EGFR sdAbs were conjugated to each Co_3O_4 NH on average.

3.8. IHC assay

EGFR is overexpressed in many solid tumors, which is closely related to tumor cell proliferation, angiogenesis, tumor invasion and metastasis and apoptosis inhibition [36,37]. Many EGFR targeted drugs have been developed, such as gefitinib, erlotinib, nimotuzumab, cetuximab and strastuzumab [38,39]. Therefore, effective detection of EGFR has the vital clinical significance. The obtained Co_3O_4 nanoprobes were applied to EGFR detection of NSCLC tissues with treatment procedures shown in Scheme 2. Fig. 2a demonstrates the membrane of EGFR overexpressed NSCLC cells with large nucleuses in the tissue were stained brown, indicating EGFR on the membrane were captured by the Co_3O_4 nanoprobes, hence the Co_3O_4 NHs were fixed in the corresponding regions, which catalyzed the oxidation of DAB by H_2O_2. As shown in Fig. 2b, before incubating with Co_3O_4 nanoprobes, the tissue was blocked with EGFR sdAb of high concentration, slight brown shown in the tissue could be derived from the nonspecific adsorption of Co_3O_4 nanoprobes. Fig. 2c shows the tissue incubated with sole Co_3O_4 NHs and slight nonspecific adsorption was also been observed. No apparent stained region was detected in EGFR negative tissue after incubating with Co_3O_4 nanoprobes (Fig. 2d). These IHC results indicate the as-obtained Co_3O_4 nanoprobes have high sensitivity and specificity for EGFR detection.

4. Conclusions

In this study, we successfully synthesized Co_3O_4 nanopolyhedrons, nanocubes, nanoplates and nanorods. It is evident that the exposed crystal planes of these NPs are very important to their peroxidase- and catalase-like activities. The specific exposure of crystal planes with higher density of Co^{3+} provides higher activity. Furthermore, Co_3O_4 NHs with smaller size and higher activity were selected to establish EGFR targeted nanoprobes. The Co_3O_4 nanoprobes were obtained by simply blending Co^{2+} coupled Co_3O_4 NHs with His-Tag fused EGFR sdAbs. This method has several advantages compared to the conventional conjugation methods. Firstly, the obtained Co_3O_4 nanoprobes have low tendency to aggregate and to cross-link during the conjugation, resulting in good stability. Secondly, the His-Tag labeled at the C-terminal of EGFR sdAb assured fully exposure of the active N-terminal domain site. IMAC is a traditional and ancient technique, basing on which we developed a new type of coupling method of NPs and antibodies. The obtained Co_3O_4 nanoprobes showed outstanding sensitivity and specificity and may find potential applications in biotechnology.

Conflict of interest

The authors declare no competing financial interest.

Acknowledgements

This research was supported by the National Important Science Research Program of China (Nos. 2011CB933503, 2013CB733800), National Natural Science Foundation of China (Nos. 81571806, 61601227, 81301870), the Basic Research Program of Jiangsu Province (Natural Science Foundation, Nos. BK2011036, BK20160939), Research Fund for the Doctoral Program of Higher Education of China (20110092110029).

Appendix A. Supplementary data

Supplementary data associated with this article can be found, in the online version, at http://dx.doi.org/10.1016/j.colsurfb.2017.02.034.

References

[1] K.M. Bratlie, C.J. Kliewer, G.A. Somorjai, Structure effects of benzene hydrogenation studied with sum frequency generation vibrational spectroscopy and kinetics on Pt (111) and Pt (100) single-crystal surfaces, J. Phys. Chem. B 110 (2006) 17925–17930.
[2] N. Tian, Z.-Y. Zhou, S.-G. Sun, Y. Ding, Z.L. Wang, Synthesis of tetrahexahedral platinum nanocrystals with high-index facets and high electro-oxidation activity, Science 316 (2007) 732–735.
[3] R. Narayanan, M.A. El-Sayed, Shape-dependent catalytic activity of platinum nanoparticles in colloidal solution, Nano Lett. 4 (2004) 1343–1348.
[4] R. Xu, D. Wang, J. Zhang, Y. Li, Shape-dependent catalytic activity of silver nanoparticles for the oxidation of styrene, Chem. Asian J. 1 (2006) 888–893.
[5] H.-X. Mai, L.-D. Sun, Y.-W. Zhang, R. Si, W. Feng, H.-P. Zhang, H.-C. Liu, C.-H. Yan, Shape-selective synthesis and oxygen storage behavior of ceria nanopolyhedra, nanorods, and nanocubes, J. Phys. Chem. B 109 (2005) 24380–24385.
[6] K. Zhou, X. Wang, X. Sun, Q. Peng, Y. Li, Enhanced catalytic activity of ceria nanorods from well-defined reactive crystal planes, J. Catal. 229 (2005) 206–212.
[7] Y. Zheng, Y. Cheng, Y. Wang, F. Bao, L. Zhou, X. Wei, Y. Zhang, Q. Zheng, Quasicubic α-Fe2O3 nanoparticles with excellent catalytic performance, J. Phys. Chem. B 110 (2006) 3093–3097.
[8] B.M. Choudary, R.S. Mulukutla, K.J. Klabunde, Benzylation of aromatic compounds with different crystallites of MgO, J. Am. Chem. Soc. 125 (2003) 2020–2021.
[9] C.C. Ge, G. Fang, X.M. Shen, Y. Chong, W.G. Wamer, X.F. Gao, Z.F. Chai, C.Y. Chen, J.J. Yin, Facet energy versus enzyme-like activities: the unexpected protection of Palladium nanocrystals against oxidative damage, Acs Nano 10 (2016) 10436–10445.
[10] T. He, D. Chen, X. Jiao, Y. Wang, Y. Duan, Solubility-controlled synthesis of high-quality Co3O4 nanocrystals, Chem. Mater. 17 (2005) 4023–4030.
[11] L. Hu, Q. Peng, Y. Li, Selective synthesis of Co_3O_4 nanocrystal with different shape and crystal plane effect on catalytic property for methane combustion, J. Am. Chem. Soc. 130 (2008) 16136–16137.
[12] J. Dong, L. Song, J.-J. Yin, W. He, Y. Wu, N. Gu, Y. Zhang, Co_3O_4 nanoparticles with multi-enzyme activities and their application in immunohistochemical assay, ACS Appl. Mater. Interfaces 6 (2014) 1959–1970.
[13] S. Muyldermans, C. Cambillau, L. Wyns, Recognition of antigens by single domain antibody fragments: the superfluous luxury of paired domains, Trends Biochem. Sci. 26 (2001) 230–235.
[14] A. Bell, Z.J. Wang, M. Arbabi-Ghahroudi, T.T.A. Chang, Y. Durocher, U. Trojahn, J. Baardsnes, M.L. Jaramillo, S.H. Li, T.N. Baral, M. O'Connor-McCourt, R. MacKenzie, J.B. Zhang, Differential tumor-targeting abilities of three single-domain antibody formats, Cancer Lett. 289 (2010) 81–90.

[15] R. Pirker, J.R. Pereira, J. von Pawel, M. Krzakowski, R. Ramlau, K. Park, F. de Marinis, W.E.E. Eberhardt, L. Paz-Ares, S. Storkel, K.M. Schumacher, A. von Heydebreck, I. Celik, K.J. O'Byrne, EGFR expression as a predictor of survival for first-line chemotherapy plus cetuximab in patients with advanced non-small-cell lung cancer: analysis of data from the phase 3 FLEX study, Lancet Oncol. 13 (2012) 33–42.
[16] V. Cortez-Retamozo, M. Lauwereys, G.H. Gh, M. Gobert, K. Conrath, S. Muyldermans, P. De Baetselier, H. Revets, Efficient tumor targeting by single-domain antibody fragments of camels, Int. J. Cancer 98 (2002) 456–462.
[17] M.M. Harmsen, H.J. De Haard, Properties, production, and applications of camelid single-domain antibody fragments, Appl. Microbiol. Biotechnol. 77 (2007) 13–22.
[18] X. Wang, G. Lu, Y. Zeng, X. Hu, L. Chen, Studies on the nanocrystalline Co_3O_4 by wet synthesis and its microstructure, Acta Chim. Sinica 61 (2003) 1849–1853.
[19] R. Xu, H.C. Zeng, Dimensional control of cobalt-hydroxide-carbonate nanorods and their thermal conversion to one-dimensional arrays of Co_3O_4 nanoparticles, J. Phys. Chem. B 107 (2003) 12643–12649.
[20] S. Shibata, M. Furukawa, Y. Ishiguro, S. Sasaki, 4-[(5-chloro-2-pyridyl) AZO]-1, 3-diaminobenzene as a new sensitive and selective reagent for cobalt, Anal. Chim. Acta 55 (1971) 231–237.
[21] E. Kiss, Pyridylazo-diaminobenzenes as reagents for cobalt: spectrophotometric determination of cobalt in silicates and meteorites, Anal. Chim. Acta 66 (1973) 385–396.
[22] S.-H. Cha, J. Hong, M. McGuffie, B. Yeom, J.S. VanEpps, N.A. Kotov, Shape-dependent biomimetic inhibition of enzyme by nanoparticles and their antibacterial activity, ACS Nano 9 (2015) 9097–9105.
[23] W. Zhang, S. Hu, J.J. Yin, W. He, W. Lu, M. Ma, N. Gu, Y. Zhang, Prussian blue nanoparticles as multienzyme mimetics and reactive oxygen species scavengers, J. Am. Chem. Soc. 138 (2016) 5860–5865.
[24] H.Z. Sha, Z.Y. Zou, K. Xin, X.Y. Bian, X.T. Cai, W.G. Lu, J. Chen, G. Chen, L. Huang, A.M. Blair, P. Cao, B.R. Liu, Tumor-penetrating peptide fused EGFR single-domain antibody enhances cancer drug penetration into 3D multicellular spheroids and facilitates effective gastric cancer therapy, J. Controlled Release 200 (2015) 188–200.
[25] N. Keloglu, B. Verrier, T. Trimaille, J. Sohiera, Controlled association and delivery of nanoparticles from jet-sprayed hybrid microfibrillar matrices, Colloids Surf. B 140 (2016) 142–149.
[26] E.W. Deutsch, C.A. Ball, J.J. Berman, G.S. Bova, A. Brazma, R.E. Bumgarner, D. Campbell, H.C. Causton, J.H. Christiansen, F. Daian, D. Dauga, D.R. Davidson, G. Gimenez, Y.A. Goo, S. Grimmond, T. Henrich, B.G. Herrmann, M.H. Johnson, M. Korb, J.C. Mills, A.J. Oudes, H.E. Parkinson, L.E. Pascal, N.I. Pollet, J. Quackenbush, M. Ramialison, M. Ringwald, D. Salgado, S.A. Sansone, G. Sherlock, C.J. Stoeckert, J. Swedlow, R.C. Taylor, L. Walashek, A. Warford, D.G. Wilkinson, Y. Zhou, L.I. Zon, A.Y. Liu, L.D. True, Minimum information specification for in situ hybridization and immunohistochemistry experiments (MISFISHIE), Nat. Biotechnol. 26 (2008) 305–312.
[27] L. Wan, M. Sun, G.J. Liu, C.C. Wei, E.B. Zhang, R. Kong, T.P. Xu, M.D. Huang, Z.X. Wang, Long noncoding RNA PVT1 promotes non-small cell lung cancer cell proliferation through epigenetically regulating LATS2 expression, Mol. Cancer Ther. 15 (2016) 1082–1094.
[28] M. Casas-Cabanas, G. Binotto, D. Larcher, A. Lecup, V. Giordani, J.M. Tarascon, Defect chemistry and catalytic activity of nanosized Co_3O_4, Chem. Mater. 21 (2009) 1939–1947.
[29] X.B. Lu, G.F. Zou, J.H. Li, Hemoglobin entrapped within a layered spongy Co_3O_4 based nanocomposite featuring direct electron transfer and peroxidase activity, J. Mater. Chem. 17 (2007) 1427–1432.
[30] G. Binotto, D. Larcher, A.S. Prakash, R.H. Urbina, M.S. Hegde, J.M. Tarascon, Synthesis, characterization, and li-electrochemical performance of highly porous Co_3O_4 powders, Chem. Mater. 19 (2007) 3032–3040.
[31] Y.L. Li, J.Z. Zhao, Y. Zhao, X.L. Hao, Z.Y. Hou, Facile solution-based synthesis and optical properties of Co_3O_4 nanoparticles at low-temperature, Chem. Res. Chin. Univ. 29 (2013) 1040–1044.
[32] M. Grzelczak, J.S. Zhang, J. Pfrommer, J. Hartmann, M. Driess, M. Antonietti, X.C. Wang, Electro- and photochemical water oxidation on ligand-free Co_3O_4 nanoparticles with tunable sizes, ACS Catal. 3 (2013) 383–388.
[33] X.L. Xiao, X.F. Liu, H. Zhao, D.F. Chen, F.Z. Liu, J.H. Xiang, Z.B. Hu, Y.D. Li, Facile shape control of Co_3O_4 and the effect of the crystal plane on electrochemical performance, Adv. Mater. 24 (2012) 5762–5766.
[34] D.W. Su, S.X. Dou, G.X. Wang, Single crystalline Co_3O_4 nanocrystals exposed with different crystal planes for Li-O_2 batteries, Sci. Rep. 4 (2014).
[35] J. Porath, J. Carlsson, I. Olsson, G. Belfrage, Metal chelate affinity chromatography, a new approach to protein fractionation, Nature 258 (1975) 598–599.
[36] U.R. Michaelis, B. Fisslthaler, M. Medhora, D. Harder, I. Fleming, R. Busse, Cytochrome P450 2C9-derived epoxyeicosatrienoic acids induce angiogenesis via cross-talk with the epidermal growth factor receptor (EGFR), FASEB J. 17 (2003) 770–772.
[37] A.K. Larsen, D. Ouaret, K. El Ouadrani, A. Petitprez, Targeting EGFR and VEGF (R) pathway cross-talk in tumor survival and angiogenesis, Pharmacol. Ther. 131 (2011) 80–90.
[38] J. Baselga, The EGFR as a target for anticancer therapy—focus on cetuximab, Eur. J. Cancer 37 (2001) 16–22.
[39] J.G. Paez, P.A. Jänne, J.C. Lee, S. Tracy, H. Greulich, S. Gabriel, P. Herman, F.J. Kaye, N. Lindeman, T.J. Boggon, EGFR mutations in lung cancer: correlation with clinical response to gefitinib therapy, Science 304 (2004) 1497–1500.